SUPPLEMENTAL INFORMATION

Condensin promotes the juxtaposition of DNA flanking its loading site in *Bacillus subtilis*

Xindan Wang, Tung B. K. Le, Bryan R. Lajoie, Job Dekker, Michael T. Laub and David Z. Rudner

This PDF file includes:

Supplemental Methods
Supplemental Tables
Supplemental References
Supplemental Figure Legends
Supplemental Figures S1-S10

Supplemental Methods.

Generation of Hi-C contact maps.

Paired-end sequencing reads were mapped independently to the genome of *Bacillus subtillis* PY79 (NCBI Reference Sequence: NC_022898.1) using Bowtie 2.1.0 and an algorithm that iteratively increases truncation length to maximize yield of valid Hi-C interactions (Imakaev et al. 2012). The iterative mapping procedure starts at a read length of 25 bp and increases in steps of 5 bp to a maximal read length of 50 bp. Only read pairs for which both reads uniquely aligned to the genome were considered in subsequent steps. The *B. subtillis* PY79 genome was divided into restriction fragments (2398 HindIII fragments) and each read of a read pair was sorted into its corresponding restriction fragment. Read pairs were classified as valid Hi-C products, non-ligation, or self-ligation products (Imakaev et al. 2012); only valid Hi-C products were considered below.

To create interaction matrices, the *B. subtillis* PY79 genome was first divided into 404 10-kb bins. Valid Hi-C products were then assigned to individual bins (Le et al. 2013). Interactions of a bin with itself, and with neighboring bins were discarded. For the presentation of the matrices, three discarded diagonals were later given the maximal cut-off value of 0.01. Raw Hi-C contact maps can be biased due to the uneven distribution of restriction enzyme sites and, to a lesser extent, differences in GC content and the mappability of individual reads (Yaffe and Tanay 2011; Imakaev et al. 2012). We therefore normalized raw contact maps using an iterative normalization procedure, implemented using the hiclib library for Python (https://bitbucket.org/mirnylab/hiclib) (Imakaev et al. 2012; Le et al. 2013). Essentially, we converted the number of interactions, or read counts, into Hi-C scores by applying the following equation and iteratively repeating it for the resulting contact map after each cycle: mij =mij * (total reads) / (total reads in bin i * total reads in bin j) (Imakaev et al. 2012). The iterative procedure was repeated until the maximum relative error of the total number of Hi-C scores in a bin was less than 10^{-5}. Resulting matrices were normalized so that Hi-C scores for each row and column sum to 1. Subsequent analysis and visualization was done using R scripts.

Identification of chromosomal interaction domains (CIDs).

We divided the *B. subtillis* PY79 genome into 10-kb bins and the contact map was represented as a matrix of interactions between bins (404x404 bin-to-bin interactions). CIDs appear as squares along the lower left to upper right diagonal of the Hi-C contact map. We rotated contact maps 45 degrees clockwise so that CIDs appear as triangles. This procedure facilitated visual representation and determination of CIDs. For each CID, the bin at the left-most edge interacted more frequently with bins to its right than to its left. Conversely, the bin at the right-most edge interacted preferentially with bins to its left. Bins within a CID interacted approximately equally with bins to the left and right. Thus, bins or loci near the edge of CIDs exhibited a preferred direction of interaction whereas those within a CID did not.

To facilitate CID assignment, we used a metric called directional preference (Dixon et al. 2012; Le et al. 2013). Briefly, to quantify the degree of directional preference for a given bin, we extracted the vector of interactions between that bin and bins at regular 10-kb intervals, either to the left or right, up to 100 kb. We then compared $\log_2$(Hi-C scores) of the two vectors by a paired t-test to assess whether the strength of interactions were significantly stronger in one direction compared to the other (Fig. S2). The more significant the difference is, the higher the absolute t-value is. Negative t-value indicated a bin is interacting more with bins to the left than to the right, and vice versa. Directional preferences for each bin along the chromosome were then represented as a bar plot with positive and negative t-values shown as red and green bars respectively. A P-value of 0.05 (represented by horizontal black dashed lines in Fig. S2) was used as a threshold to assess statistical significance. At CID boundaries the directional preference of bins changed most dramatically (Fig. S2). Bins near the middle of a CID also changed their preferred direction but did so more gradually than those at the boundaries. CID boundary assignments for wild-type was aided by using the directional preference plot of a G1-arrested *dnaBts* strain, in which CIDs are more pronounced (Fig. S2C).

To identify the genes that are highly expressed in our growth condition (exponential growth in CH medium at 37˚C), we first obtained gene expression data from transcription profiles (Nicolas et al. 2012) and shortlisted genes with absolute expression value ≥ 15 (165 genes). We further filtered by gene length and kept only genes whose length is ≥ 1000 bp (leaving 46 genes). Genomic locations of these 46 genes were converted from *B. subtilis* 168 genome coordinates (NCBI Reference Sequence: NC_000964) to PY79 coordinates (NC_022898.1) using their accompanying protein tables. The position of these highly transcribed genes are represented as orange dashed lines on top of the Hi-C contact maps (Fig. S2). Separately, the start position of the 10 *rrn* operons were represented as black dashed lines.

Correlation analyses.

Pearson correlation coefficients between Hi-C experiments were carried out as follows (Le et al. 2013). The main diagonal, as well as 20 sub- and super-diagonals of the two-dimensional matrices representing Hi-C contact maps, were removed to prevent over-representation of high intra-chromosomal-arm interactions that might dominate the correlation analyses. The resulting matrices were then decomposed to one-dimensional vectors row-by-row. R was used to compute the Pearson correlation coefficient (*r*) and to plot scatter graph between vectors (Fig. S4).

Image analysis.

Image analyses were performed using the MATLAB-based program, MicrobeTracker (Sliusarenko et al. 2011). Vegetatively growing cells form septated chains (Fig. 1B). The outline of individual cells was determined using cytoplasmic mCherry, expressed under the control of a constitutive promoter, P_{veg} (Fukushima et al. 2003). The background fluorescence intensity was determined by averaging the fluorescence intensity in cell-free regions of the image and subtracted from the image in MetaMorph. After background subtraction, the images were inverted and analyzed using built-in algorithms in

MicrobeTracker. For each cell, a co-ordinate system called a mesh was generated, in which each point in the cell was described by two co-ordinates: the distance to a cell pole that was randomly selected and the distance to the mid-line along the cell length. The mesh was used to calculate cell parameters such as the length, width, and area.

The number and cellular position of chromosomal loci was detected using SpotFinder in MicrobeTracker and recorded into the cell mesh (Fig. 1CD, Fig. S3CDF, S8CD). To determine inter-focal distance (d) between a pair of mYpet (a) and CFP (b) foci, only cells with equal number of foci in the two fluorescence channels were analyzed (Fig. 1B). The foci were paired according to their distance from a pole randomly determined by the software. For instance, a1 is paired with b1, and a2 with b2 (Fig. 1B). The distance (d) between each pair of foci was measured, binned with 0.1 µm (Fig. 1CD, Fig. S3CDF) or 0.05 µm (Fig. S8CD) increments and plotted. The x-axis shows the inter-focal distance in µm. The y-axis represents the percentage of foci pairs with an inter-focal distance falling into each bin. A two-sample Kolmogorov-Smirnov test was performed in MatLab and a P-value was returned.

Immunoblot analysis.

Cells were induced for sporulation by resuspension (Harwood and Cutting 1990). After 1 hour, OD_{600} was measured and 1 ml of cells were collected and resuspended in lysis buffer [20 mM Tris pH 7.0, 10 mM EDTA, 1 mg/ml lysozyme, 10 µg/ml DNase I, 100 µg/ml RNase A, with protease inhibitors: 1 mM PMSF, 1 µg/ml leupeptin, 1 µg/ml pepstatin] to a final OD_{600} of 10 for equivalent loading. The cells were incubated at 37˚C for 10 min followed by addition of equal volume of sodium dodecyl sulfate (SDS) sample buffer [0.25 M Tris pH 6.8, 4% SDS, 20% glycerol, 10 mM EDTA] containing 10% 2-Mercaptoethanol. Samples were heated for 5 min at 80˚C prior to loading. Proteins were separated by SDS-PAGE on 15% polyacrylamide gels, electroblotted onto Immobilon-P membranes (Millipore) and blocked in 5% nonfat milk in phosphate-buffered saline (PBS)-0.5% Tween-20. The blocked membranes were probed with anti-GFP (1:10,000) (Rudner et al. 1999), anti-Spo0J

(1:5,000) (Lin et al. 1997), anti-SMC (1:5000) (Lindow et al. 2002), anti-SigA (1:10,000) (Fujita 2000) or anti-SigF (1:5000) (Pan et al. 2001) diluted into 3% BSA in 1x PBS-0.05% Tween-20. Primary antibodies were detected using horseradish peroxidase-conjugated goat anti-rabbit IgG (BioRad) and the Super Signal chemiluminscence reagent as described by the manufacturer (Pierce).

Plasmid construction.

pBT02 [+4˚ *metS (wt parS)* in pMiniMAD *erm*] was generated by inserting the region containing the wild-type *parS* site between *metS* and *yabD* (amplified using odr526 and odr529 from the wild-type genomic DNA, and digested using EcoRI and BamHI) into the pMiniMAD plasmid between EcoRI and BamHI. The pMiniMAD plasmid was a gift from Dan Kearns, Indiana University.

pBT08 [-1˚ *parB (wt parS)* in pMiniMAD *erm*] was generated by inserting the region containing the wild-type *parS* site in the *parB* gene (amplified using oWX1094 and 1095 from wild-type genomic DNA, and digested using EcoRI and BamHI) into the pMiniMAD plasmid between EcoRI and BamHI.

pBT10 [*Δsoj132* no a.b. in pMiniMAD *erm*] was generated by inserting the region containing the in frame deletion of *parA*, called *Δsoj132* (amplified using oWX1104 and 1105 from strain SV132 (Lee and Grossman 2006) , and digested using EcoRI and BamHI) into the pMiniMAD plasmid between EcoRI and BamHI.

pER74 [*sacA::*P_{veg}*-mCherry erm*] was generated by releasing the phleomycin resistance gene from pER69 [*sacA::*P_{veg}*-mCherry phleo*] (Meisner et al. 2013) using BamHI and SalI, and replacing it with erythromycin resistance gene liberated from pKM82 using BamHI and SalI.

pWX571 [*scpB-mgfpmut3 erm*] was constructed by inserting *scpB*$_{Cter}$*-mgfpmut3* fragment (liberated from pWX530 using EcoRI and HindIII) into pWX442 between EcoRI and HindIII. pWX530 [*scpB-mgfpmut3 cat*] was built by successive cloning steps with *scpB*$_{Cter}$ (no stop codon) originally amplified from wild-type genomic DNA using odr780 and 781, and *mgfpmut3* originally amplified from pDHL580 (Landgraf et al. 2012) using oWX671 and 672. pWX442 is a cloning vector containing erythromycin resistance gene.

pWX599 [*pelB::P*$_{soj}$ *mcherry-parB(ΔparS) cat*] was constructed by 3-way ligation to insert *mcherry* (amplified from pDR201 using oWX774 and 775 and digested with HindIII and XhoI), and *parB (ΔparS)* (liberated with XhoI and BamHI from pKM256 [*pelB::P*$_{soj}$*-gfp-parB (ΔparS) cat*](Sullivan et al. 2009)), into pKM170 between HindIII and BamHI. pKM170 was built by inserting the promoter of *parA (P*$_{soj}$) (amplified from wild-type genomic DNA using odr470 and 471 and digested with EcoRI and HindIII) into pKM20 between EcoRI and HindIII. pKM20 [*pelB::cat*] is an ectopic integration vector for double crossover insertions into the *pelB* locus (K. Marquis and D.Z.R., unpublished).

pWX600 [*pelB::P*$_{soj}$ *mcherry-parB1(Vc) cat*] was built the same way as pWX599, except that *parB1* from *Vibrio cholerae* (Vc) was cloned instead of *parB (ΔparS). parB1(Vc)* was amplified using oWX1062 and 1063 from pMF392 [*pBAD33 yfp-parB1(Vc)*] (Yamaichi et al. 2007).

pWX680 [*ykoW::parA-parB-yyaC erm*] was built by cloning the *parA-parB-yyaC* region (amplified from wild-type genomic DNA using primers oWX1211 and 1212 and digested with EcoRI and BamHI) into pWX104 [*ykoW::erm*] between EcoRI and BamHI. pWX104 is an ectopic integration vector for double crossover insertions into the *ykoW* locus (X.W. and D.Z.R., unpublished).

Strain construction.

ΔparA (Δsoj132) no a.b.. The unmarked in frame deletion of *ΔparA* (*Δsoj132* (Lee and Grossman 2006)) in BWX2876 was introduced by allelic replacement using single cross-over integration plasmid pBT10, which is based on a derivative of pMAD (Arnaud et al. 2004) called pMiniMAD (a gift from Dan Kearns, Indiana University). Essentially, pBT10 was transformed to wild-type strain PY79 and selected on MLS plate. Transformants were grown in liquid culture in the absence of MLS selection to allow for "loop-out" of the plasmid. The culture was plated after serial dilution and individual colonies were screened for loss of MLS resistance. As the resulting MLS sensitive clones can either contain the mutation of interest (in this case, *Δsoj132*) or reverse to the wild-type, those clones were further analyzed by PCR and sequencing using primers oWX507 and 508.

-1˚ *parB* (*wt parS*). Using the same pMiniMAD allelic replacement method described above, the wild-type *parS* site at -1˚ (in *parB*) was introduced back to the strain that lacks all 8 origin proximal *parS* sites, *parSΔ8* (BNS1657 (Sullivan et al. 2009)), using pBT08. The *parS* was amplified from MLS sensitive clones using oWX507 and 508 and sequenced using oWX508. The correct clone was named BDR2996.

+4˚ *metS* (*wt parS*). Similarly, the wild-type *parS* site at +4˚ (between *metS* and *yabD*) was introduced back to *parSΔ8* using pBT02. From MLS sensitive clones, the *parS* site was amplified using odr530 and 531 and sequenced using oWX1099. The strain that contain a wild-type *parS* site is named BDR2985.

***parSΔ9*.** The strain that lacks 9 *parS* sites (*parSΔ9* spec, BWX3196) was constructed by deleting the *parS* site at +91˚ (in *yhaX*) from *parSΔ8* (BNS1657 (Sullivan et al. 2009)), a strain that lacks the 8 origin proximal *parS* sites. The endogenous +91˚ *parS* site (AGTTCCACATGAAACG) was deleted by direct transformation of an isothermal assembly (Gibson et al. 2009) product into BNS1657. The isothermal reaction contained 3 PCR fragments: 1) region upstream of the *parS* site (amplified from the wild-type genomic DNA using oWX1233 and 1234); 2) *loxP-spec-loxP* cassette (amplified from pWX466 using

universal primers oWX438 and 439) and 3) a region downstream of the *parS* site (amplified from wild-type genomic DNA using primers oWX1235 and 1236). pWX466 contains a *loxP-spec-loxP* cassette (X.W. and D.Z.R., unpublished). The transformants was PCR amplified using oWX1237 and 1238, and the *parS* deletion was sequenced using oWX1237. The resulting construct (BWX3196) had the center 12 bp of the *parS* site deleted, which also confers a 4 amino acid deletion at the C-terminus of the YhaX protein. Using the same method, *parSΔ9 loxP-kan-loxP* (BWX3198) was built with the antibiotic cassette amplified from pWX470. The *loxP-kan-loxP* cassette was subsequently looped out using a *cre*-expressing plasmid pDR244, which contains a spectinomycin resistance gene and a temperature sensitive replication origin, generating an unmarked strain with 9 *parS* sites deleted (BWX3212*, parSΔ9 no a.b.*).

-94˚*parS kan*. To build BWX3221, which has the +4˚ *parS* site (TGTTACACGTGAAACA) inserted at -94˚ (in the intergenic region between *ytaB* and *glgP*) in *parSΔ9* spec (BWX3196), an isothermal assembly product was directly transformed to BWX3196. The isothermal assembly reaction contains 3 PCR products: 1) a region containing *ytaB* gene (amplified from wild-type genomic DNA using oWX1239 and 1240); 2) *loxP-kan-loxP* cassette flanked by the +4˚ *parS* site (amplified from pWX470 using universal primers oWX1241 and oWX438) and 3) the region containing *glgD* (amplified from wild-type genomic DNA using primers oWX1242 and 1243). Genomic DNA was extracted from the transformants and the region flanking the *parS* site was amplified and sequenced using oWX1244 and 1245. As an intermediate strain towards BWX3231 (see below), the same isothermal assembly product was also transformed to *parSΔ8*, resulting in strain BWX3217 (*parSΔ8*, -94˚ *parS kan*), which was confirmed by PCR and sequencing.

+91˚*parS* spec. We sought to obtain a counterpart of -94˚*parS kan* on the opposing arm, that is to insert the same +4˚ *parS* site (TGTTACACGTGAAACA) at +91˚. Since there is a weak endogenous *parS* site (AGTTCCACATGAAACG) at +91˚ inside *yhaX* gene, we deleted it and inserted the +4˚ *parS* site, downstream of *yhaX* gene. This construct (BWX3231) was

built by direct transformation of an isothermal assembly reaction into BWX3217. The isothermal assembly reaction contains 2 PCR products: 1) the upstream piece containing *yhaX(ΔparS)* (amplified using oWX1233 and oWX1246 from BWX3196); and 2) a PCR product containing the +4˚ *parS* site, *loxP-spec-loxP* cassette and the region down stream of *yhaX* (amplified using oWX1241 and oWX1236 from BWX3196). The transformants were amplified and sequenced using oWX1237 and 1238. The resulting construct removes the endogenous *parS* site from *yhaX* gene and inserts the +4˚ *parS* site down stream of *yhaX*.

***smc (wt) spec*.** The spectinomycin resistance gene was inserted down stream of the *smc* gene to serve as a matched wild-type control for *smcts* mutants that are linked to the same resistance marker (Fig. 3A). This construct was obtained by direct transformation of an isothermal assembly reaction that contained 3 PCR products: 1) the 3' half of the *smc* gene (1.2 kb) amplified using oWX848 and 849 from wild-type genomic DNA. 2) a spectinomycin resistance cassette (amplified from pWX466 using oWX823 and oWX438) and 3) a 2.2 kb fragment downstream of the *smc* gene (amplified from wild-type genomic DNA using oWX850 and 851. The insertion was confirmed by PCR and sequencing using oWX852 and oAM97. The resulting strain is BWX2080.

Supplemental Table 1. Strains used in this study.

strain	genotype	reference	figure
PY79	*wild-type*	(Youngman et al. 1983)	1A, 3D
BDR1873	*ΔparAB::spec*	(Graham et al. 2014)	1A
BWX1912	*yuxG(-87˚)::lacO48 (phleo), yhdG(+87˚)::tetO48 (cat), ycgO::PftsW tetR-cfp (kan) terminators PftsW lacI-mypet, sacA::P_{veg}-mCherry (erm)*	this study	1BC
BWX3168	*yuxG(-87˚)::lacO48 (phleo), yhdG(+87˚)::tetO48 (cat), ycgO::PftsW tetR-cfp (kan) terminators PftsW lacI-mypet, sacA::P_{veg}-mCherry (erm), ΔparAB::spec*	this study	1C
BWX3248	*lacA(-64˚)::lacO120 (phleo), yrvN(-125˚)::tetO48 (cat), ycgO::PftsW tetR-cfp (kan) terminators PftsWlacI-mYpet, sacA::P_{veg}-mCherry (erm)*	this study	1D
BWX3446	*lacA(-64˚)::lacO120 (phleo), yrvN(-125˚)::tetO48 (cat), ycgO::PftsW tetR-cfp (kan) terminators PftsWlacI-mYpet, sacA::P_{veg}-mCherry (erm), ΔparAB::spec*	this study	1D
BWX2876	*ΔparA (Δsoj132) no a.b.*	this study	2A
BDR2292	*ΔparB::spec*	(Ireton et al. 1994)	2A
BWX3196	*parSΔ9 (spec): parSΔ8, +91˚ yhaX (ΔparS) (spec)*	this study	2A
BDR2707	*pelB::P_{soj} parA-parB G77S (ΔparS) (cat), ΔparAB::spec*	this study	2A
BWX3208	*ΔparB::spec, pelB::P_{soj} mcherry-parB(ΔparS) (cat)*	this study	2BDE
BWX3209	*ΔparB::spec, pelB::P_{soj} mcherry-parB1(Vc) (cat)*	this study	2BDE
BWX2519	*parSΔ8, pelB::P_{soj} mcherry-parB(ΔparS) (cat)*	this study	2B
BWX2520	*parSΔ8, pelB::P_{soj} mcherry-parB1(Vc) (cat)*	this study	2B
BWX2514	*ΔparB::spec, scpB-mgfpmut3 (erm), pelB::P_{soj} mcherry-parB(ΔparS) (cat)*	this study	2C
BWX2515	*ΔparB::spec, scpB-mgfpmut3 (erm), pelB::P_{soj} mcherry-parB1(Vc)(cat)*	this study	2C
BWX2030	*scpB-mgfpmut3 (erm)*	this study	2C
BWX2049	*ΔparB::spec, scpB-mgfpmut3 (erm)*	this study	2C
BWX3151	*smcts02 (spec)*	(Wang et al. 2014b)	3A
BWX2080	*smc (wt) (spec)*	this study	3A
BWX3266	*spoIIIE36, smcts02 (spec)*	this study	3C
BDR2298	*Δsmc::neo*	(Britton et al. 1998)	3D
BWX941	*yycR(-7˚)::tetO48 (cat), ycgO::PftsW tetR-cfp (phleo), scpB-yfp (spec)*	this study	4A
BWX3327	*ΔparAB::cat, scpB-yfp (spec)*	this study	4AB
BKM1634	*scpB-yfp (spec)*	(Sullivan et al. 2009)	4B
BDR2996	*parSΔ8, -1˚ parB (wt parS)*	this study	5A
BDR2985	*parSΔ8, +4˚ metS (wt parS)*	this study	5A
BNS1657	*parSΔ8: parB (parSΔ), yycG (parSΔ) , rocR (parSΔ), cotF (parSΔ), metS (parSΔ), ybbC(parSΔ), ydaD(parSΔ), nfrA(parSΔ)*	(Sullivan et al. 2009)	5C
BWX2761	*parSΔ8, ΔparB (ΔparS)::spec*	this study	5C
BDR3007	*parSΔ8, ΔparA (Δsoj132 no a.b.)*	this study	5C
BWX3304	*parSΔ8, smcts02 (spec)*	this study	5D
BWX3172	*ykoW (+122˚)::parA-parB-yyaC (erm)*	this study	5E
BWX3359	*parSΔ9 no.a.b., -94˚parS no a.b., smcts02 (spec)*	this study	5F
BWX3231	*parSΔ9 no.a.b., -94˚parS (kan), +91˚parS (spec)*	this study	5G
BWX2533	*yycR (-7˚)::tetO48 (cat), ycgO::PftsW tetR-cfp (phleo), dnaX-yfp (spec), dnaB134 (ts) - zhb83::Tn917 (erm)*	this study	6A
BNS1733	*dnaB134 (ts) - zhb83::Tn917 (erm)*	(Rokop et al. 2004)	6B
AG1468	*Δspo0J::spec, trpC2, pheA1*	(Ireton et al. 1994)	

AG1505	*Δ(soj spo0J)::spec, trpC2, pheA1*	(Ireton et al. 1994)
BWX2538	*Δsoj132 spec, trpC2, pheA1*	(Wang et al. 2014b)
BWX3198	*parSΔ9 (kan): parSΔ8, +91˚ yhaX (ΔparS) (kan)*	this study
BWX3212	*parSΔ9 no.a.b.*	this study
BWX3217	*parSΔ8, -94˚parS (kan)*	this study
BWX3221	*parSΔ9 (spec), -94˚parS (kan)*	this study
DCL468	*spo0J (ΔparS), trpC2, pheA1*	(Lin and Grossman 1998)
JH693	*spo0J93, trpC2, pheA1*	(Hoch and Mathews 1973)
KPL69	*trpC2, pheA1, dnaB134 (ts) - zhb83::Tn917 (erm)*	(Rokop et al. 2004)
RB35	*Δsmc::neo, trpC2, pheA1*	(Britton et al. 1998)
spoIIIE36	*spoIIIE36*	(Wu and Errington 1994)
SV132	*trpC2, pheA1, Δsoj132 (no a.b.)*	(Lee and Grossman 2006)

Supplemental Table 2. Plasmids used in this study.

plasmid	description	reference
pBT02	+4˚ *metS (wt parS)* in pMiniMAD (*erm*)	this study
pBT08	-1˚ *parB (wt parS)* in pMiniMAD (*erm*)	this study
pBT10	*ΔparA (Δsoj132 no a.b.)* in pMiniMAD (*erm*)	this study
pER74	*sacA::*P_{veg}*-mcherry (erm)*	this study
pTG123	*pelB::*P_{soj} *parA-parB G77S (ΔparS) (cat)*	(Graham et al. 2014)
pWX154	*yhdG (+87˚)::tetO48 (cat)*	(Wang et al. 2014a)
pWX159	*yuxG (-87˚)::lacO48 (phleo)*	(Wang et al. 2014a)
pWX425	*ycgO::PftsW tetR-cfp (kan) terminators PftsW lacI-mYpet*	(Wang et al. 2014a)
pWX571	*scpB-mgfpmut3 (erm)*	this study
pWX599	*pelB::*P_{soj} *mcherry-parB(ΔparS) (cat)*	this study
pWX600	*pelB::*P_{soj} *mcherry-parB1(Vc) (cat)*	this study
pWX680	*ykoW (+122˚)::parA-parB-yyaC (erm)*	this study

Supplemental Table 3. Oligonucleotides used in this study.

oligos	sequence	use
oAM97	cacgaacgaaaatcgccattc	BWX2080
odr470	gccGAATTCaatccggctttaatgatcagat	pWX599
odr471	cgccAAGCTTtcacatgaacatgtactatct	pWX599
odr526	cgcGAATTCagccagaatcacgcaaaaacgaaatg	pBT02
odr529	cgcGGATCCgcctccttctcctcggagag	pBT02
odr530	ggaaatacgcggatcgtcttctg	BDR2985
odr531	cgtcagctcatgagccgcgtacg	BDR2985
odr780	cgcGAATtctttagaagtactggccattg	pWX571
odr781	cggCTCGAGttttatatcttcgaaggtttggttaaag	pWX571
oWX438	gaccagggagcactggtcaac	universal
oWX439	tccttctgctccctcgctcag	universal
oWX507	cgtgcttgaattttcaattatttccc	BWX2876, BDR2996, BDR3019
oWX508	acccgttgcaaaggctcactgggcgc	BWX2876, BDR2996, BDR3019
oWX671	aaaCTCGAGggatctggcggatcaggcatgagtaaaggagaagaacttttcactgg	pWX571
oWX672	cgcGGATCCAAGCTTttactatttgtatagttcatccatgccatg	pWX571
oWX774	cgcAAGCTTacataaggaggaactactatggtc	pWX599
oWX775	tttCTCGAGtccggaacctttgtataattcgtccattccacc	pWX599
oWX823	cagtaacgaggaaagaggttaaaagggatccttctgctccctcgctcag	BWX2080
oWX848	gaagagctctctgccgtatctgaaaag	BWX2080
oWX849	ctgagcgagggagcagaaggatccctttttaacctctttcctcgttac	BWX2080
oWX850	gttgaccagtgctccctggtctaacgaggaaagaggttaaaagatgagc	BWX2080
oWX851	cgtcagcctcaagcagcgcaagacgg	BWX2080
oWX1062	gcgCTCGAGatgactaaacgtggtttaggaaaaggg	pWX600
oWX1063	cgcGGATCCttagttttgcagcttggcaatcag	pWX600
oWX1094	gcgGAATTCagtatataagacagttattccgcg	pBT08
oWX1095	tttGGATCCgtttcacatacagatgctgcagcggc	pBT08
oWX1099	gcaaattgacctctttcgctaaggcg	BDR2985
oWX1104	cgcGAATTctgataatatattgtgatggcatggcg	pBT10
oWX1105	tttGGATCCgccaagaagcgtgcgtccatgtccc	pBT10
oWX1211	cgcGAATTCgtttccacgttctgtactgtgacttc	pWX680
oWX1212	cgcGGATCCaaagttcagcttgttcccgttattg	pWX680
oWX1233	tattgattcttcccaatgcgctaaccc	BWX3196; BWX3231
oWX1234	ctgagcgagggagcagaaggactcgagttacacacgcttatcaagaaatccttttcgc	BWX3196
oWX1235	gttgaccagtgctccctggtcaaaagccgctcgcgccctgacaggtgc	BWX3196
oWX1236	gcactgtaatcagtgctgctttgtcg	BWX3196; BWX3231
oWX1237	cggcttcttcacgaaaagtattcc	BWX3196; BWX3231
oWX1238	tttatgaagcagctttgtgggccg	BWX3196; BWX3231
oWX1239	caaccgcttcgaggtagatttgaatgg	BWX3221
oWX1240	tgtttcacgtgtaacactcgagtcacagattcattgaattgattg	BWX3221
oWX1241	ctcgagtgttacacgtgaaacatccttctgctccctcgctcag	BWX3221; BWX3231
oWX1242	gttgaccagtgctccctggtcacaaaaaaagccgcttatacagcg	BWX3221
oWX1243	aatgcggatcaagcagtggacgtgccg	BWX3221
oWX1244	gataaagggtaattaaatacatgcgg	BWX3221
oWX1245	atgaacggggctttgacgatcggc	BWX3221
oWX1246	tgtttcacgtgtaacactcgagttacacacgcttatcaagaaatc	BWX3231

Restriction endonuclease sites are capitalized.

Supplemental References

Arnaud M, Chastanet A, Debarbouille M. 2004. New vector for efficient allelic replacement in naturally nontransformable, low-GC-content, gram-positive bacteria. *Applied and environmental microbiology* **70**: 6887-6891.

Britton RA, Lin DC, Grossman AD. 1998. Characterization of a prokaryotic SMC protein involved in chromosome partitioning. *Genes Dev* **12**: 1254-1259.

Dixon JR, Selvaraj S, Yue F, Kim A, Li Y, Shen Y, Hu M, Liu JS, Ren B. 2012. Topological domains in mammalian genomes identified by analysis of chromatin interactions. *Nature* **485**: 376-380.

Fujita M. 2000. Temporal and selective association of multiple sigma factors with RNA polymerase during sporulation in Bacillus subtilis. *Genes Cells* **5**: 79-88.

Fukushima T, Ishikawa S, Yamamoto H, Ogasawara N, Sekiguchi J. 2003. Transcriptional, functional and cytochemical analyses of the veg gene in Bacillus subtilis. *J Biochem* **133**: 475-483.

Gibson DG, Young L, Chuang RY, Venter JC, Hutchison CA, 3rd, Smith HO. 2009. Enzymatic assembly of DNA molecules up to several hundred kilobases. *Nat Methods* **6**: 343-345.

Graham TG, Wang X, Song D, Etson CM, van Oijen AM, Rudner DZ, Loparo JJ. 2014. ParB spreading requires DNA bridging. *Genes Dev* **28**: 1228-1238.

Harwood CR, Cutting SM. 1990. *Molecular Biological Methods for Bacillus*. Wiley, New York.

Hoch JA, Mathews JL. 1973. Chromosomal location of pleiotropic negative sporulation mutations in Bacillus subtilis. *Genetics* **73**: 215-228.

Imakaev M, Fudenberg G, McCord RP, Naumova N, Goloborodko A, Lajoie BR, Dekker J, Mirny LA. 2012. Iterative correction of Hi-C data reveals hallmarks of chromosome organization. *Nat Methods* **9**: 999-1003.

Ireton K, Gunther NW, Grossman AD. 1994. spo0J is required for normal chromosome segregation as well as the initiation of sporulation in Bacillus subtilis. *J Bacteriol* **176**: 5320-5329.

Landgraf D, Okumus B, Chien P, Baker TA, Paulsson J. 2012. Segregation of molecules at cell division reveals native protein localization. *Nat Methods* **9**: 480-482.

Le TB, Imakaev MV, Mirny LA, Laub MT. 2013. High-resolution mapping of the spatial organization of a bacterial chromosome. *Science* **342**: 731-734.

Lee PS, Grossman AD. 2006. The chromosome partitioning proteins Soj (ParA) and Spo0J (ParB) contribute to accurate chromosome partitioning, separation of replicated sister origins, and regulation of replication initiation in Bacillus subtilis. *Mol Microbiol* **60**: 853-869.

Lin DC, Grossman AD. 1998. Identification and characterization of a bacterial chromosome partitioning site. *Cell* **92**: 675-685.

Lin DC, Levin PA, Grossman AD. 1997. Bipolar localization of a chromosome partition protein in Bacillus subtilis. *Proc Natl Acad Sci U S A* **94**: 4721-4726.

Lindow JC, Kuwano M, Moriya S, Grossman AD. 2002. Subcellular localization of the Bacillus subtilis structural maintenance of chromosomes (SMC) protein. *Mol Microbiol* **46**: 997-1009.

Marbouty M, Cournac A, Flot JF, Marie-Nelly H, Mozziconacci J, Koszul R. 2014. Metagenomic chromosome conformation capture (meta3C) unveils the diversity of chromosome organization in microorganisms. *eLife* **3**: e03318.

Meisner J, Montero Llopis P, Sham LT, Garner E, Bernhardt TG, Rudner DZ. 2013. FtsEX is required for CwlO peptidoglycan hydrolase activity during cell wall elongation in Bacillus subtilis. *Mol Microbiol* **89**: 1069-1083.

Nicolas P, Mader U, Dervyn E, Rochat T, Leduc A, Pigeonneau N, Bidnenko E, Marchadier E, Hoebeke M, Aymerich S et al. 2012. Condition-dependent transcriptome reveals high-level regulatory architecture in Bacillus subtilis. *Science* **335**: 1103-1106.

Pan Q, Garsin DA, Losick R. 2001. Self-reinforcing activation of a cell-specific transcription factor by proteolysis of an anti-sigma factor in B. subtilis. *Mol Cell* **8**: 873-883.

Rokop ME, Auchtung JM, Grossman AD. 2004. Control of DNA replication initiation by recruitment of an essential initiation protein to the membrane of Bacillus subtilis. *Mol Microbiol* **52**: 1757-1767.

Rudner DZ, Fawcett P, Losick R. 1999. A family of membrane-embedded metalloproteases involved in regulated proteolysis of membrane-associated transcription factors. *Proc Natl Acad Sci U S A* **96**: 14765-14770.

Sliusarenko O, Heinritz J, Emonet T, Jacobs-Wagner C. 2011. High-throughput, subpixel precision analysis of bacterial morphogenesis and intracellular spatio-temporal dynamics. *Mol Microbiol* **80**: 612-627.

Sullivan NL, Marquis KA, Rudner DZ. 2009. Recruitment of SMC by ParB-parS organizes the origin region and promotes efficient chromosome segregation. *Cell* **137**: 697-707.

Umbarger MA, Toro E, Wright MA, Porreca GJ, Bau D, Hong SH, Fero MJ, Zhu LJ, Marti-Renom MA, McAdams HH et al. 2011. The three-dimensional architecture of a bacterial genome and its alteration by genetic perturbation. *Mol Cell* **44**: 252-264.

Wang X, Montero Llopis P, Rudner DZ. 2014a. Bacillus subtilis chromosome organization oscillates between two distinct patterns. *Proc Natl Acad Sci U S A*.

Wang X, Tang OW, Riley EP, Rudner DZ. 2014b. The SMC condensin complex is required for origin segregation in Bacillus subtilis. *Curr Biol* **24**: 287-292.

Wu LJ, Errington J. 1994. Bacillus subtilis spoIIIE protein required for DNA segregation during asymmetric cell division. *Science* **264**: 572-575.

Yaffe E, Tanay A. 2011. Probabilistic modeling of Hi-C contact maps eliminates systematic biases to characterize global chromosomal architecture. *Nature genetics* **43**: 1059-1065.

Yamaichi Y, Fogel MA, McLeod SM, Hui MP, Waldor MK. 2007. Distinct centromere-like parS sites on the two chromosomes of Vibrio spp. *J Bacteriol* **189**: 5314-5324.

Youngman PJ, Perkins JB, Losick R. 1983. Genetic transposition and insertional mutagenesis in Bacillus subtilis with Streptococcus faecalis transposon Tn917. *Proc Natl Acad Sci U S A* **80**: 2305-2309.

Supplemental Figure Legends.

Figure S1. Re-orienting the Hi-C contact map (related to Figure 1). The published Hi-C contact maps of circular genomes are plotted according to genome position (from 0 kb to 4033 kb, *ori* - *ter* - *ori*) and have the terminus region in the center of the map and the origin region at 4 corners (Umbarger et al. 2011; Le et al. 2013; Marbouty et al. 2014). To more clearly visualize the long-range interactions in the origin region, we present Hi-C contact maps with the origin at the center.

Figure S2. Chromosome interacting domains (CIDs) are largely unchanged in the absence of the *parAB* locus. (A) The Hi-C contact map for wild-type cells (grown in rich medium at 37˚C) in its traditional orientation (0 kb - 4033 kb) was rotated 45˚ clockwise to place the primary diagonal on the X-axis. Directional preference plots were generated as described in Supplemental Methods. The boundaries of the CIDs were mapped using these plots as guides and are presented as short black bars below the plots. In wild-type, we detected 25 CIDs ranging from 60 to 340 kb. 6 of the 7 *rrn* clusters coincide with a CID boundary. The locations of the highly transcribed *rrn* operons (black dotted lines) and other highly transcribed genes (orange dotted lines, see Supplemental Methods) are indicated. **(B)** The directional preference plot for cells lacking *parAB*. The short-range interactions along the genome are very similar to those in wild-type. The interactions over a large region in the terminus (centered at ~2000 kb) in the wild-type are missing in the *ΔparAB* mutant. These are inter-arm interactions at the terminus region that are absent in the Δ*parAB* mutant (Fig. 1A). **(C)** The directional preference plot for *dnaBts* after 120 min at the restrictive temperature (42˚C) (Fig. 6B). The CID boundaries are more pronounced in this condition. We detected 35 CIDs (ranging from 40 to 270 kb) of which 15 coincide with CIDs from wild-type in **(A)**.

Figure S3. Long-range chromosome interactions (related to Figure 1). (A) Interactions between a ~300 kb region spanning the origin (red) with large regions on the left and right chromosome arms (blue). Left, the location of the above mentioned regions are indicated

with red or blue bars on the x- and y-axis. Middle, the interactions are highlighted with a yellow box on the Hi-C contact map. Right, schematic representation of the long-range interactions on a circular map of the chromosome. The interacting regions (red and blue) are shown. Yellow lines indicate the interactions highlighted in the yellow box in the middle panel. Because Hi-C was performed on asynchronously growing cells, we cannot rule out the possibility that the long-range interactions detected here are between sister chromatids. However, we suspect that most interactions are intra-chromosomal because replicated DNA is rapidly resolved and segregated based on time-lapse imaging of chromosomal loci (Wang et al. 2014a). Furthermore, the Hi-C contact map of cells with 1-N chromosomal content (*dnaBts* 42˚C for 45 min) has similar interactions to the asynchronous cells (middle panels of Fig. 6B, Fig. S9B). **(B)** Long-range chromosome interactions are largely unchanged in *ΔparA* compared to the wild-type in **(A)**. **(C-D)** Distance between loci on opposing arms in cells with or without *parA* in rich **(C)** and minimal medium **(D)**. The wild-type data (light blue bars) in **(C)** are the same as the light blue bars in Fig. 1C. **(E)** Long-range chromosome interactions are lost in *ΔparAB* during growth in minimal medium. **(F)** Distance between loci on opposing arms increases in cells without *parAB* when growing in minimal medium. The wild-type data (light blue bars) are the same as the light blue bars in **(D). (G)** Long-range chromosome interactions are lost during sporulation in *ΔparAB* mutant**.** Normalized contact maps of wild-type (left) and *ΔparAB* (right) cells harvested 150 min after the initiation of sporulation (at 37˚C). Both strains contained a mutant in the SpoIIIE DNA translocase (*spoIIIE36*) that engages the chromosome after polar division but does not transport DNA (Wu and Errington 1994). The origin region appears to be insulated from the rest of the chromosome in wild-type. The molecular basis for this will be the subject of a future study.

Figure S4. Pearson correlation between Hi-C experiments. Normalized Hi-C matrices were decomposed into vectors to calculate Pearson's correlation coefficients (see Supplemental Methods). **(A)** Top, comparison of biological replicates of wild-type samples collected on different days and sequenced in different Hi-C runs. Bottom, comparison of

the wild-type with *ΔparAB* growing in rich (CH) medium (Fig. 1A). **(B)** Strains with Hi-C contact maps similar to the wild-type (*ΔparA* (Fig.2A), *dnaBts* growing at 30˚C (Fig. 6B), and mCherry-ParB(Bs) (Fig. 2E)) were compared to wild-type (top) and *ΔparAB* (bottom). **(C)** Strains with Hi-C contact maps similar to *ΔparAB* (*ΔparB* (Fig. 2A), *parSΔ9* (Fig. 2A), *parB G77S* (Fig. 2A), and mCherry-ParB1(Vc) (Fig. 2E)) were compared to wild-type (top) and *ΔparAB* (bottom). The values on the axes are Hi-C interaction scores. The two strains labeled on the x- and y-axis are compared. Pearson correlation coefficient (*r*) is indicated on each plot. Red dashed lines represent least squares best fits.

Figure S5. ChIP-seq analysis of mCherry-ParB (Bs) and mCherry-ParB1 (Vc) (related to Figure 2). (A) ChIP-seq profile of the whole genome was plotted for mCherry-ParB (Bs) (black) and mCherry-ParB1 (Vc) (blue). Number of Reads per million reads was plotted. The positions of *parS* sites are indicated (red dotted lines). **(B)** Regions spanning the 9 *parS* sites.

Figure S6. Quantification of inter-arm interactions. (A) Method to quantify total inter-arm interactions. The normalized Hi-C contact map was plotted according to genome position (0 kb to 4033 kb). The primary diagonal reporting the short-range intra-arm interactions was masked by blocking 40 bins on either side of the diagonal. On the secondary (inter-arm interaction) diagonal, a 40 bin x 40 bin region centered on the origin region was omitted from the analysis. Hi-C interaction scores between every bin with 40 bins on the opposite arm of the chromosome (within the black boxes) were summed. The ratio of inter-arm interactions to total interactions was determined for each map and reported in the bar graphs in Figures 3B and 5B. **(B)** Method to quantify interaction of two bins separated by 2000 kb (~half of a genome). A line was drawn from bin 200 (2000 kb) on the left y-axis to bin 204 (2040 kb) on the top x-axis, crossing the secondary diagonal at +90˚/-90˚ and parallel to the primary diagonal. The position of the line is shown in two contact maps (wild-type and the *ΔparAB*) as examples. The arrowheads indicate the

direction of the plot on the x-axis in **(C)**. The Hi-C interaction scores along this line were plotted for the indicated mutants in **(C).**

Figure S7. The condensin complex is less restricted to the origin region in cells with a single origin-proximal *parS* site (related to Figure 4). (A) Representative fluorescence images of mCherry-ParB and ScpB-mGFP in vegetatively growing cells. ScpB-mGFP forms clusters of foci (highlighted by yellow carets) near mCherry-ParB. **(B)** Localization of ScpB-GFP and the replication origin (*tetO*/TetR-mCherry) in wild-type, or *parSΔ9* with a single *parS* site at -1˚. ScpB-mGFP forms clusters of foci near the origin in wild-type. In the strain with a single *parS* site, ScpB-mGFP forms foci that are less restricted to the origin region than wild-type. **(C)** Localization of mGFP-ParB during sporulation. Cells were imaged 1 h after resuspension in sporulation medium. Membranes were visualized using TMA-DPH; DNA with HbsU-mCherry. Scale bars indicate 4 µm.

Figure S8. Origin-distal *parS* sites bring flanking chromosomal loci into close proximity (related to Figure 5) (A) Normalized Hi-C contact maps of cells harboring a single endogenous (weak) *parS* site at +91˚ (*parSΔ8*) (Fig. 5C), a single ectopic (strong) *parS* site at -94˚ (BWX3221, not shown in main text), or two ectopic (strong) *parS* sites at +91˚ and -94˚ (Fig. 5G). Dotted lines highlight the positions of the +91˚ and -94˚ *parS* sites (gray), the *rrn* operons (black) and the highly transcribed operon that encodes ATP synthase (red). **(B)** Re-oriented Hi-C contact maps (from the right panel of **(A)** and Fig. 5G) of cells harboring two ectopic (strong) *parS* sites at +91˚ and -94˚. The map on the left is centered on +91˚; the one on the right is centered on -94˚. Dotted lines highlight the positions of the +91˚ and -94˚ *parS* sites (gray), the indicated highly transcribed *rrn* operons (black), the operon that encodes ATP synthase (red) and the terminus region (blue). Black arrows highlight the interactions between the terminus region and two origin-proximal CIDs bounded by the indicated highly transcribed genes. **(C)** Distributions of inter-focal distances (using *tetO*/TetR-CFP and *lacO*/LacI-mYpet) between -64˚ and -125˚ loci in the presence and absence of the -94˚ *parS* site in cells grown in rich (top) and minimal

(bottom) medium. **(D)** Distributions of inter-focal distances between +54˚ and +135˚ loci in the presence and absence of the +91˚ *parS* site in cells grown in rich (top) and minimal (bottom) medium. The x-axis is the inter-focal distance in µm. The y-axis is the percentage of cells that fall in each 0.05 µm bin. P-values were calculated using two-sample Kolmogorov-Smirnov test in MatLab.

Figure S9. Long-range interactions in the origin region in cells blocked for initiation of DNA replication (related to Figure 6). (A) Representative fluorescence images showing replication origins (*tetO*/TetR-CFP, top) and replisome foci (DnaX-YFP, bottom) in *dnaBts* cells grown at 30˚C and 45 min and 120 min at 42˚C. After 45 min at 42˚C, most cells have 1-N DNA content (single origin and no replisome foci) and the chromosome is a single-lobed structure. By 120 min, the chromosome resolves into a bi-lobed structure. Scale bar indicates 4 µm. **(B)** Normalized Hi-C contact maps for the *dnaBts* strain under the same conditions. The positions of the 9 *parS* sites (gray dotted lines) and the highly transcribed *rrn* loci (black dotted lines) are indicated. The positions of the *parS* sites at -27˚, +17˚, +42˚ and +91˚ are highlighted on the x-axis. Black arrows highlight the two interaction arcs that emanate from -27˚ on the secondary diagonal. **(C)** The normalized Hi-C contact map (from the right panel of **(B)** and Fig. 6B) of *dnaBts* cells grown at 42˚C for 120 min was plotted according to genome position (0 to 4033 kb) placing the terminus in the center of the map. The terminus region between 163˚ and -177˚ (blue dotted lines) is highlighted in the right map. This region interacts with both chromosome arms.

Figure S10. Alternative model for condensin-mediated alignment (related to Figure 7). (A) Same as Figure 7Ciii, condensin is loaded onto DNA by ParB such that the ring encircles two DNA helices: one from each side of the *parS* site. As the ring slides away from the ParB/*parS* complex it tethers the flanking DNA together. **(B)** Two interacting or interlocked condensin rings topologically entrap DNA on either side of the *parS* site and these "handcuffs" similarly tether flanking DNA together as they migrate away from their loading site.

Wang_Figure S1

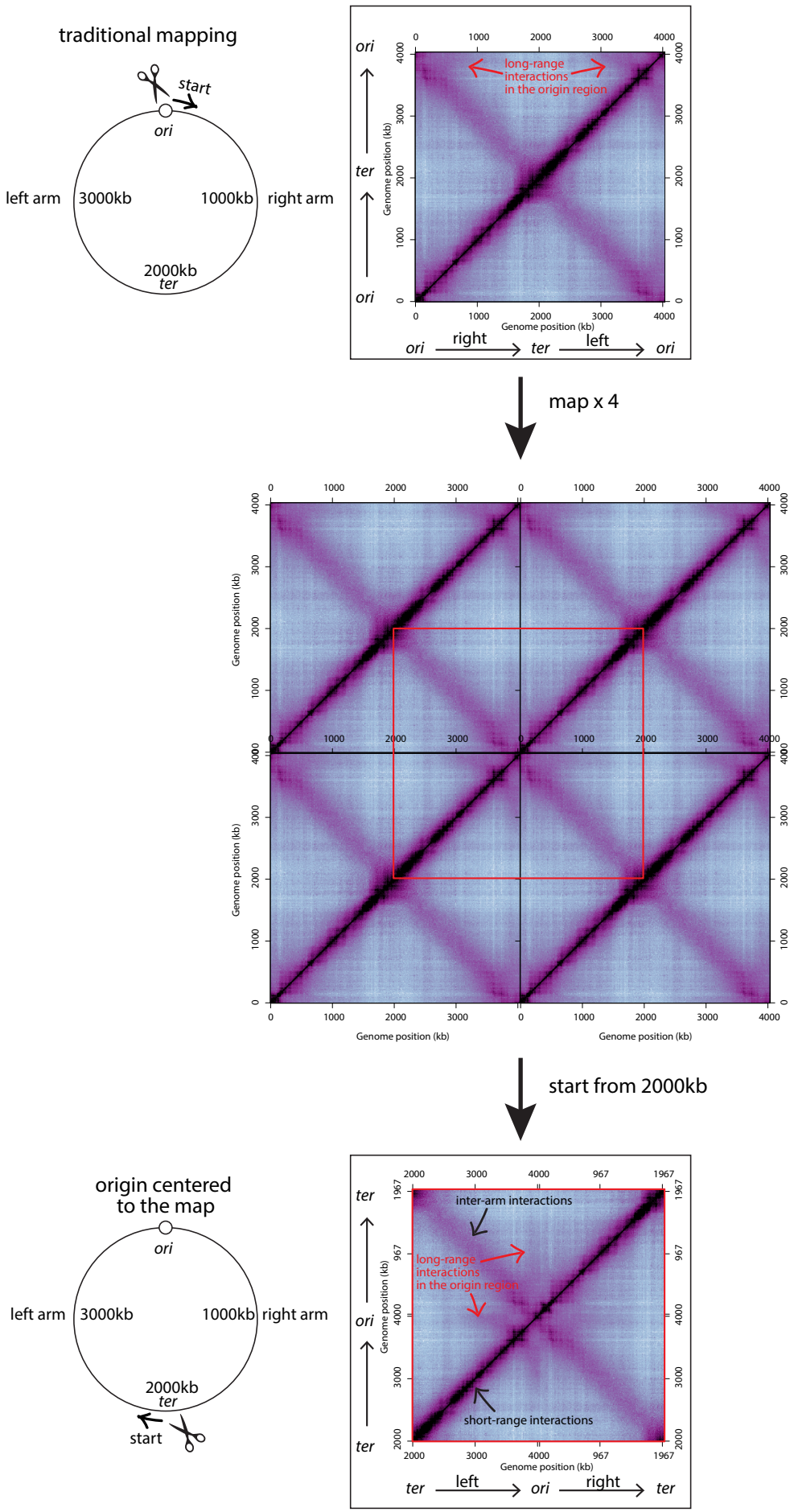

Wang_Figure S2

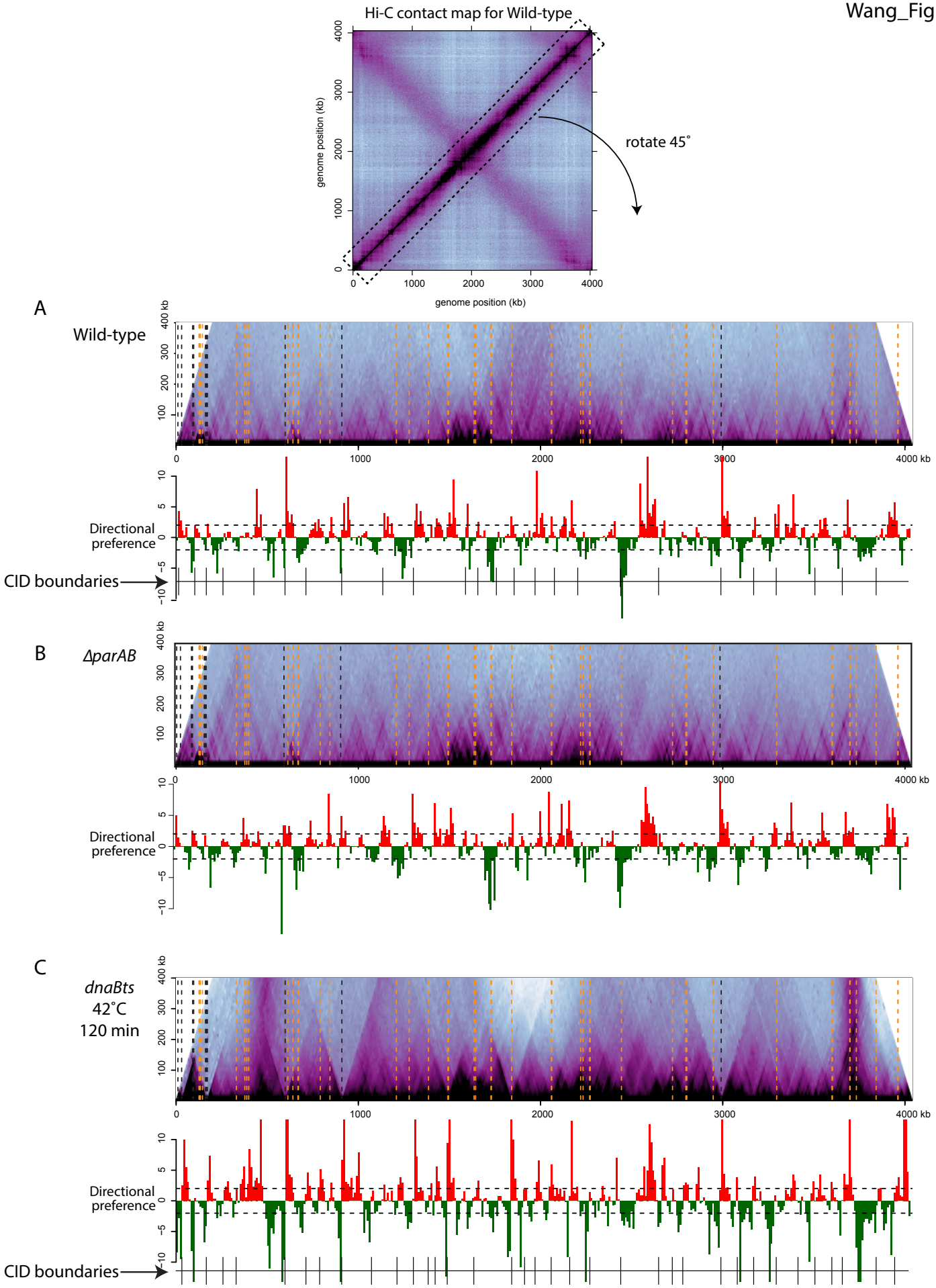

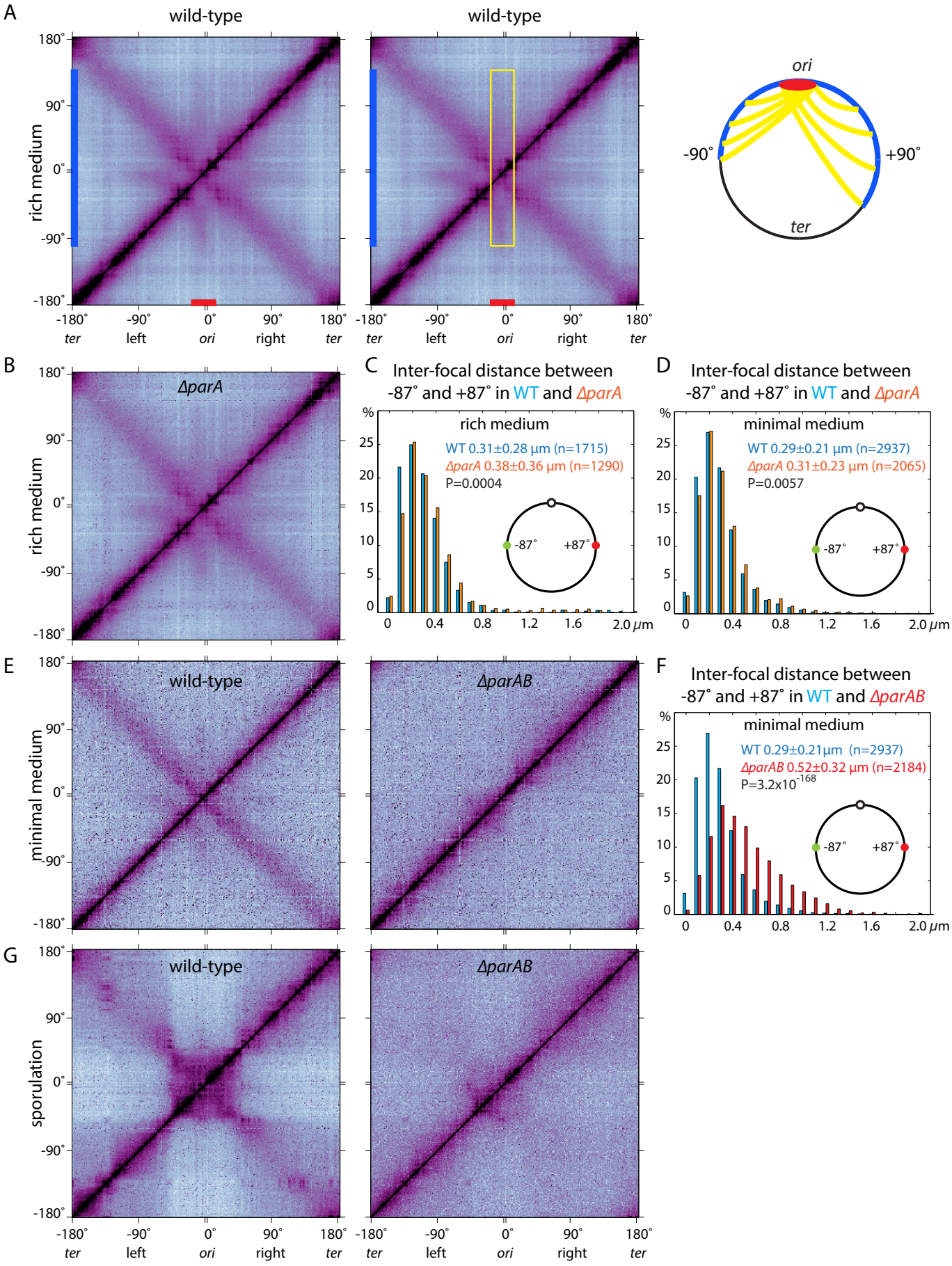
A
wild-type
wild-type
rich medium
180°
90°
0°
-90°
-180°
-180° ter
-90° left
0° ori
90° right
180° ter
ori
-90°
+90°
ter
B
ΔparA
C
Inter-focal distance between
-87° and +87° in WT and ΔparA
rich medium
WT 0.31±0.28 μm (n=1715)
ΔparA 0.38±0.36 μm (n=1290)
P=0.0004
-87°
+87°
%
2.0 μm
D
Inter-focal distance between
-87° and +87° in WT and ΔparA
minimal medium
WT 0.29±0.21 μm (n=2937)
ΔparA 0.31±0.23 μm (n=2065)
P=0.0057
E
wild-type
ΔparAB
minimal medium
F
Inter-focal distance between
-87° and +87° in WT and ΔparAB
minimal medium
WT 0.29±0.21μm (n=2937)
ΔparAB 0.52±0.32 μm (n=2184)
P=3.2x10^-168
G
wild-type
ΔparAB
sporulation

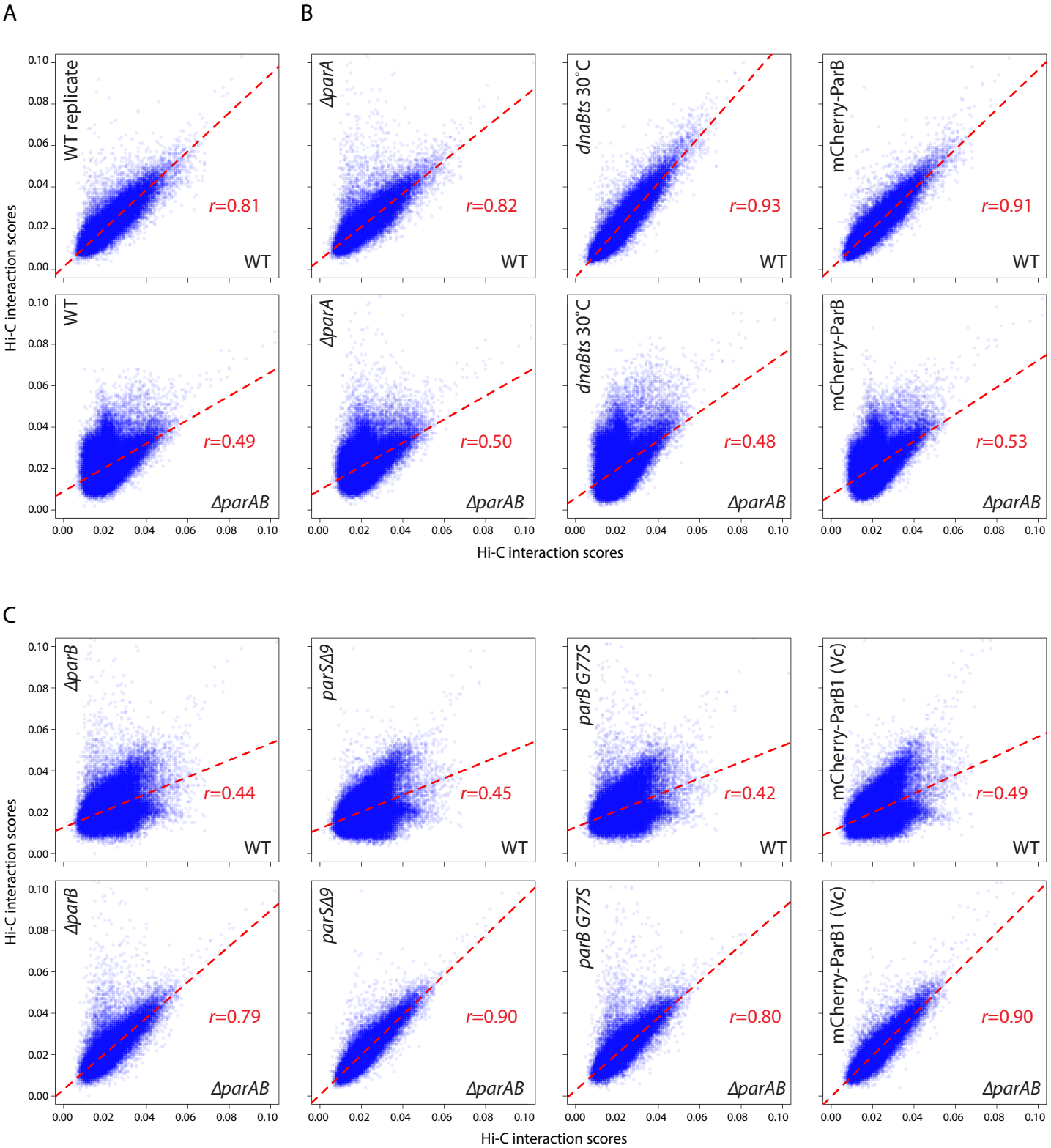
A
B
C
WT replicate
ΔparA
dnaBts 30°C
mCherry-ParB
WT
ΔparAB
ΔparB
parSΔ9
parB G77S
mCherry-ParB1 (Vc)
r=0.81
r=0.82
r=0.93
r=0.91
r=0.49
r=0.50
r=0.48
r=0.53
r=0.44
r=0.45
r=0.42
r=0.49
r=0.79
r=0.90
r=0.80
r=0.90
Hi-C interaction scores
0.00
0.02
0.04
0.06
0.08
0.10

Wang_Figure S5

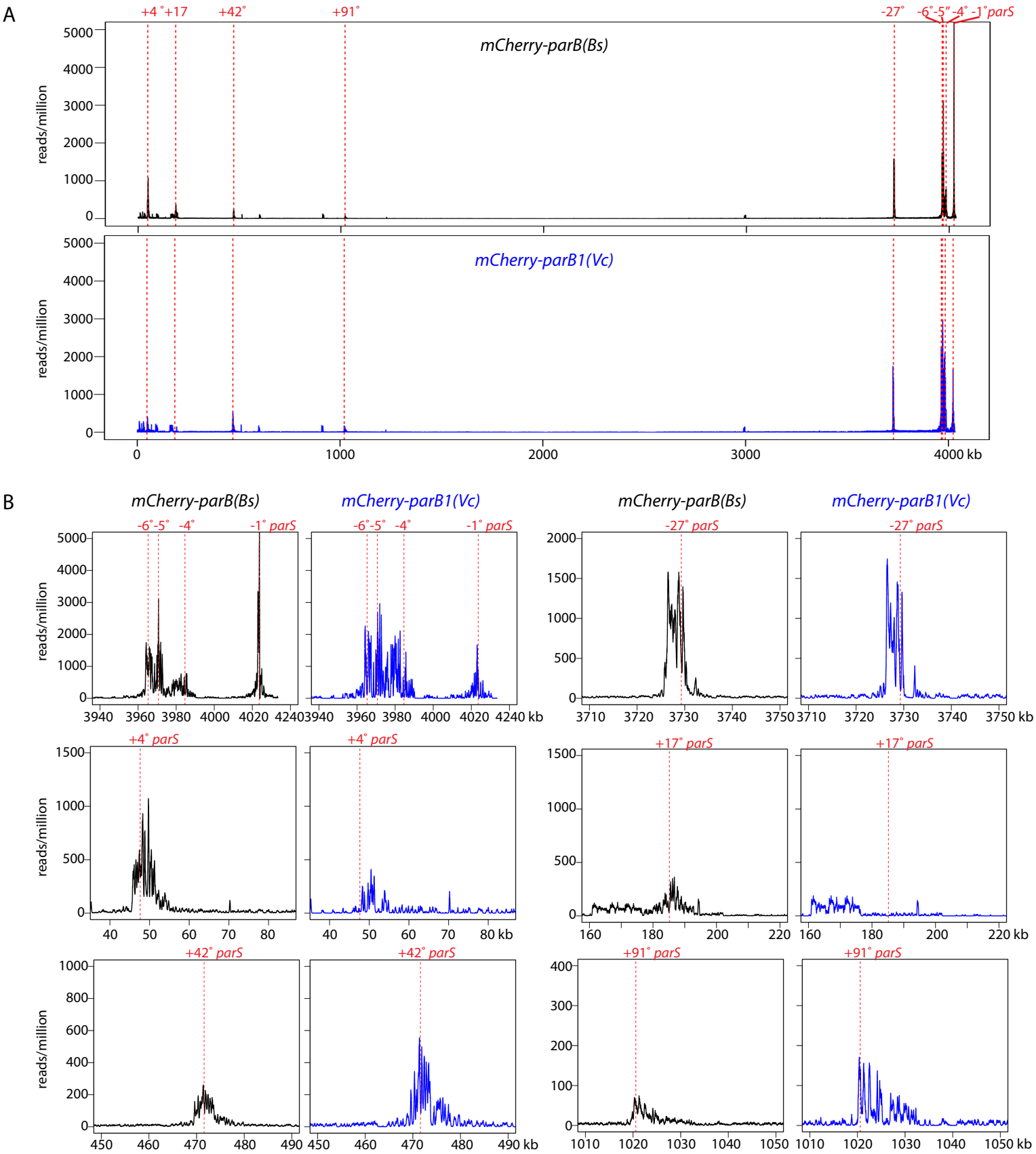

Wang_Figure S6

A

Quantification of total inter-arm interactions

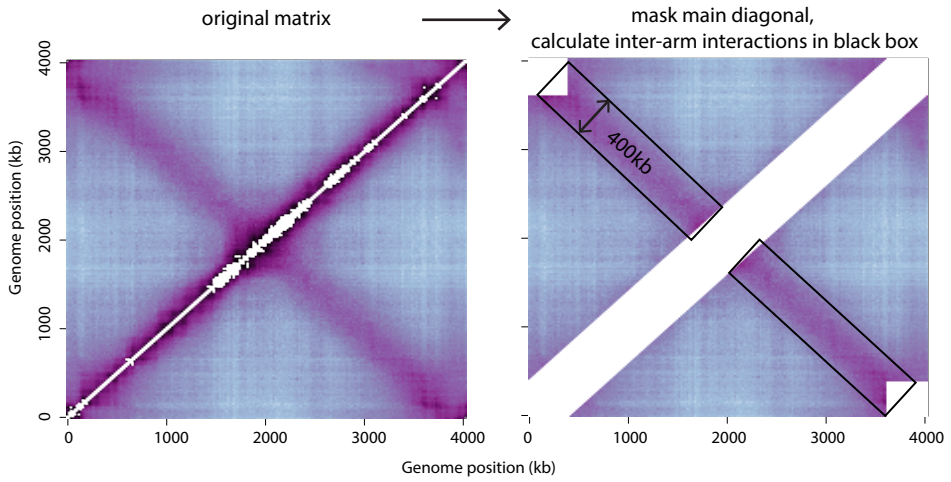

B

Slide through bin 200, parallel to the main diagonal

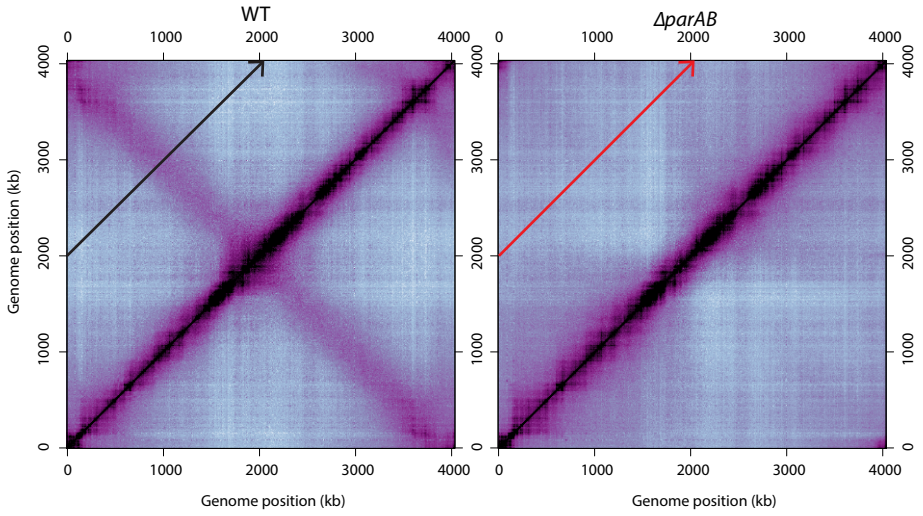

C

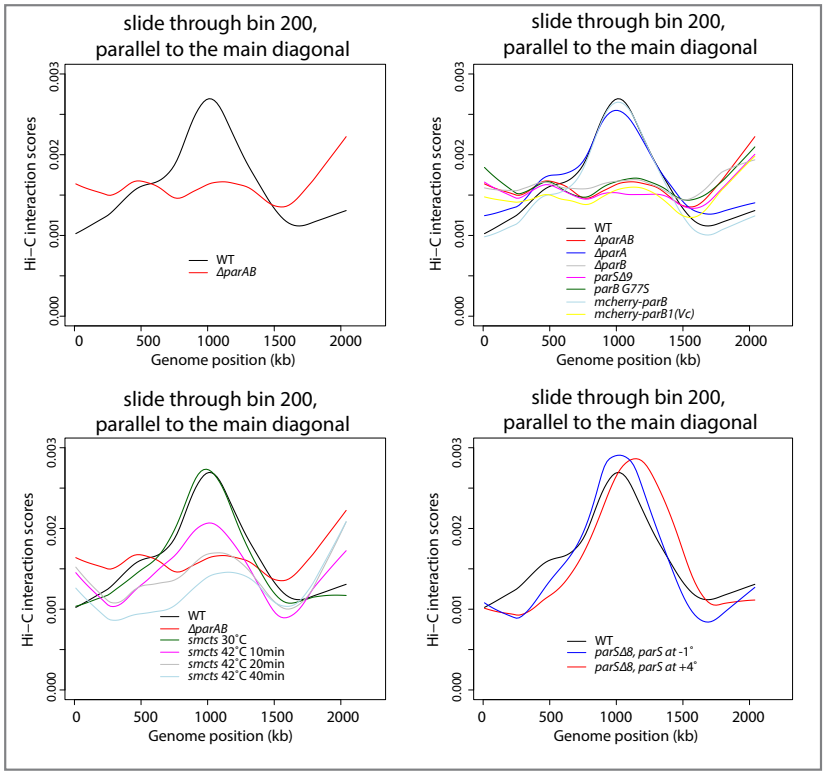

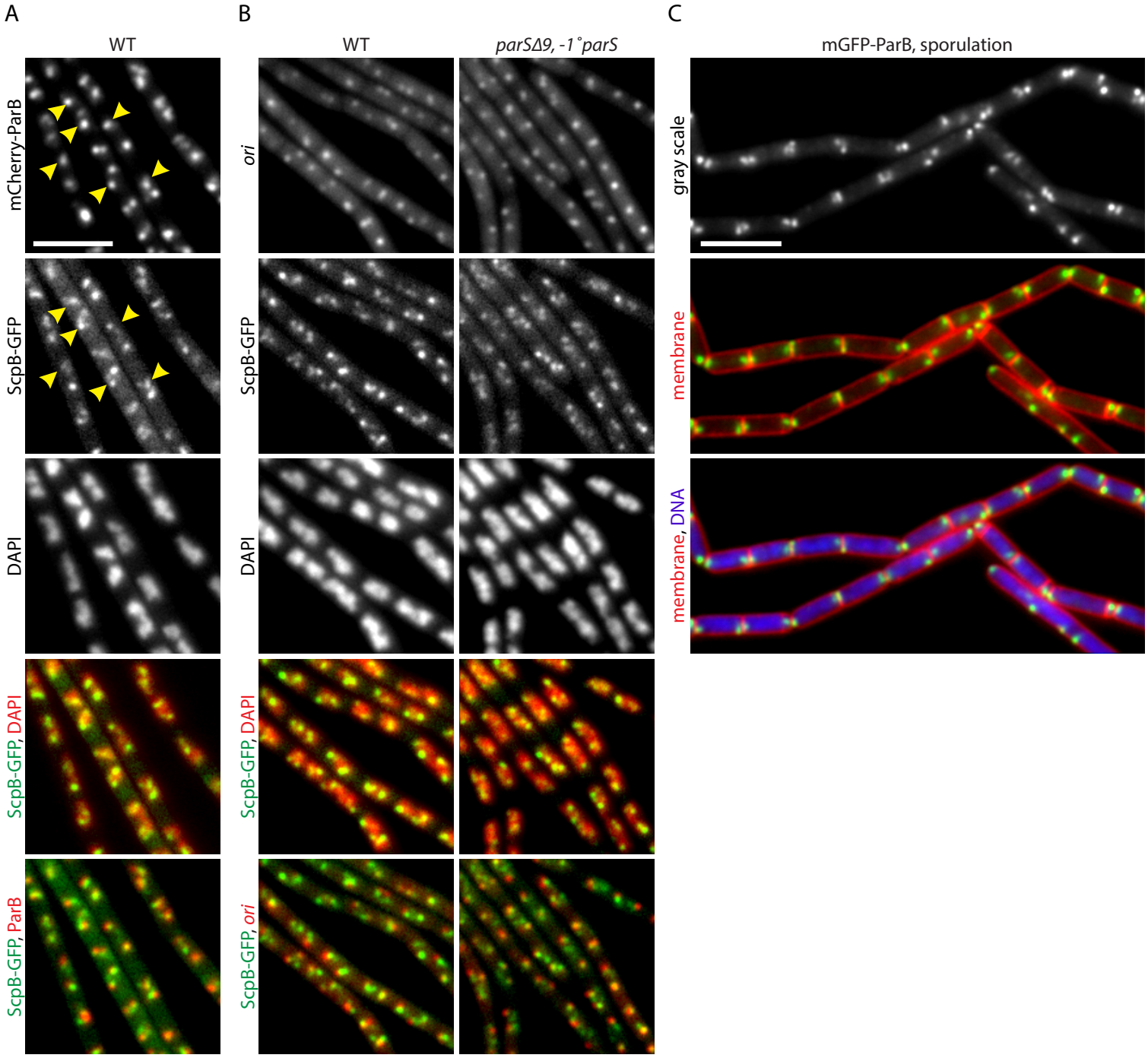
A
WT
mCherry-ParB
ScpB-GFP
DAPI
ScpB-GFP, DAPI
ScpB-GFP, ParB
B
WT
parSΔ9, -1˚parS
ori
ScpB-GFP
DAPI
ScpB-GFP, DAPI
ScpB-GFP, ori
C
mGFP-ParB, sporulation
gray scale
membrane
membrane, DNA

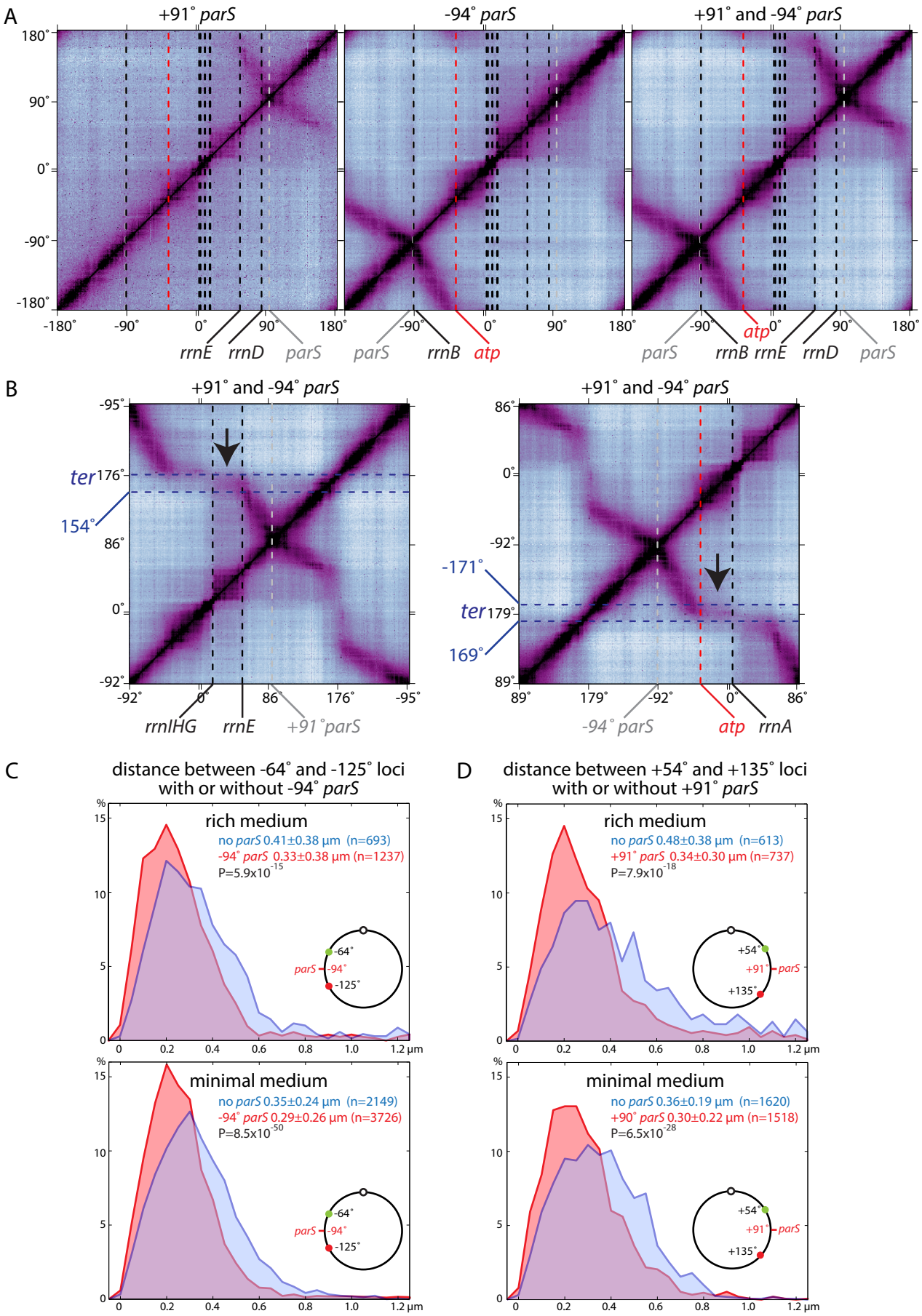
A
+91° parS
-94° parS
+91° and -94° parS
180°
90°
0°
-90°
-180°
rrnE rrnD parS
parS rrnB atp
parS rrnB rrnE rrnD parS
B
+91° and -94° parS
ter 176°
154°
86°
0°
-92°
-95°
rrnIHG rrnE +91°parS
-171°
ter 179°
169°
89°
179°
-94° parS atp rrnA
C
distance between -64° and -125° loci
with or without -94° parS
rich medium
no parS 0.41±0.38 µm (n=693)
-94° parS 0.33±0.38 µm (n=1237)
P=5.9x10^-15
minimal medium
no parS 0.35±0.24 µm (n=2149)
-94° parS 0.29±0.26 µm (n=3726)
P=8.5x10^-50
-64°
-94°
-125°
D
distance between +54° and +135° loci
with or without +91° parS
rich medium
no parS 0.48±0.38 µm (n=613)
+91° parS 0.34±0.30 µm (n=737)
P=7.9x10^-18
minimal medium
no parS 0.36±0.19 µm (n=1620)
+90° parS 0.30±0.22 µm (n=1518)
P=6.5x10^-28
+54°
+91°
+135°
%
1.2 µm

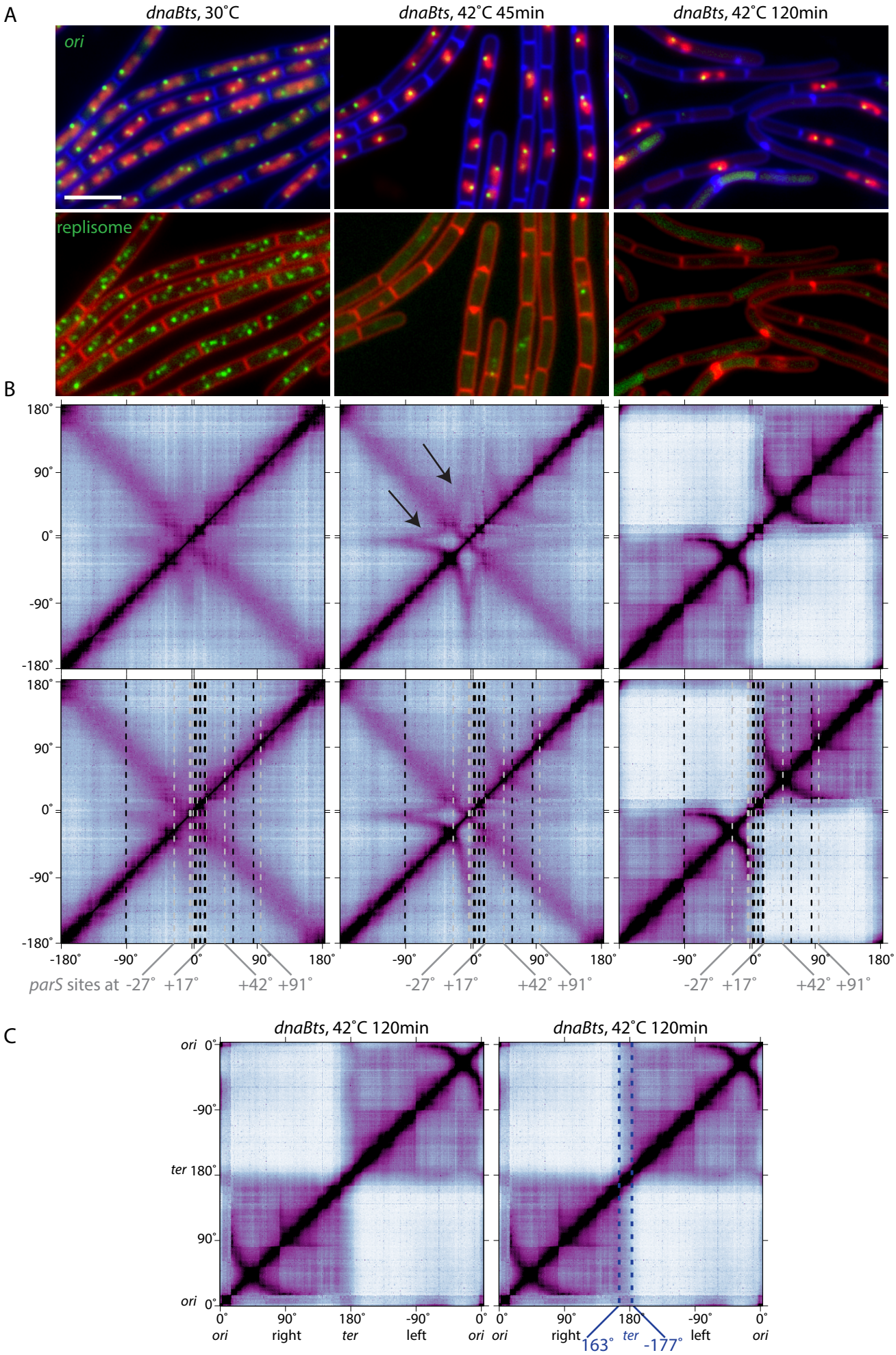
A
dnaBts, 30˚C
dnaBts, 42˚C 45min
dnaBts, 42˚C 120min
ori
replisome
B
180˚
90˚
0˚
-90˚
-180˚
parS sites at -27˚ +17˚ +42˚ +91˚
C
dnaBts, 42˚C 120min
dnaBts, 42˚C 120min
ori 0˚
-90˚
ter 180˚
90˚
ori 0˚
0˚ ori
90˚ right
180˚ ter
-90˚ left
0˚ ori
163˚
-177˚

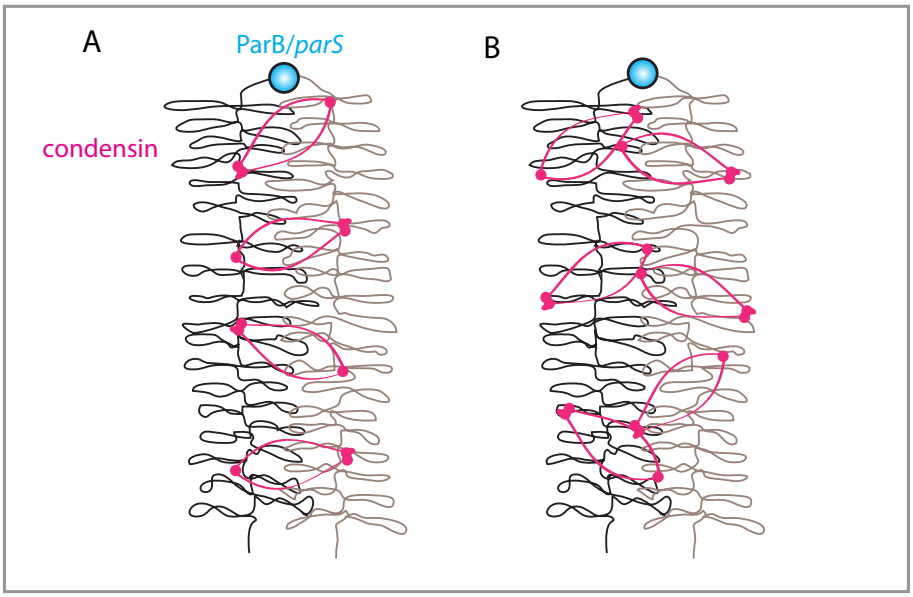
A
ParB/*parS*
condensin
B